

Article

ICESat/GLAS Data as a Measurement Tool for Peatland Topography and Peat Swamp Forest Biomass in Kalimantan, Indonesia

Uwe Ballhorn ^{1,2,*}, Juilson Jubanski ² and Florian Siegert ^{1,2}

¹ Biology Department II, GeoBio Center, Ludwig-Maximilians-University, Grosshaderner Strasse 2, D-82152 Planegg-Martinsried, Germany

² Remote Sensing Solutions GmbH, Isarstrasse 3, D-82065 München, Germany; E-Mail: jubanski@rssgmbh.de (J.J.); siegert@rssgmbh.de (F.S.)

* Author to whom correspondence should be addressed; E-Mail: ballhorn@rssgmbh.de; Tel.: +49-89-4895-4766; Fax: +49-89-4895-4767.

Received: 21 July 2011; in revised form: 22 August 2011 / Accepted: 26 August 2011 /

Published: 2 September 2011

Abstract: Indonesian peatlands are one of the largest near-surface pools of terrestrial organic carbon. Persistent logging, drainage and recurrent fires lead to huge emission of carbon each year. Since tropical peatlands are highly inaccessible, few measurements on peat depth and forest biomass are available. We assessed the applicability of quality filtered ICESat/GLAS (a spaceborne LiDAR system) data to measure peatland topography as a proxy for peat volume and to estimate peat swamp forest Above Ground Biomass (AGB) in a thoroughly investigated study site in Central Kalimantan, Indonesia. Mean Shuttle Radar Topography Mission (SRTM) elevation was correlated to the corresponding ICESat/GLAS elevation. The best results were obtained from the waveform centroid ($R^2 = 0.92$; $n = 4,186$). ICESat/GLAS terrain elevation was correlated to three 3D peatland elevation models derived from SRTM data ($R^2 = 0.90$; overall difference = -1.0 m, ± 3.2 m; $n = 4,045$). Based on the correlation of *in situ* peat swamp forest AGB and airborne LiDAR data ($R^2 = 0.75$, $n = 36$) an ICESat/GLAS AGB prediction model was developed ($R^2 = 0.61$, $n = 35$). These results demonstrate that ICESat/GLAS data can be used to measure peat topography and to collect large numbers of forest biomass samples in remote and highly inaccessible peatland forests.

Keywords: ICESat/GLAS; LiDAR; SRTM; tropical peatlands; carbon; above ground biomass; peat swamp forest; Indonesia

1. Introduction

Peatlands store huge amounts of carbon as peat consists of dead, incompletely decomposed plant material that has accumulated over thousands of years in waterlogged environments that lack oxygen. In the tropics, peatland is usually covered by forests and current estimates indicate that the total area of tropical peatland is in the range of 30–45 million ha (approximately 10–12% of the total global peatland resource); about 16.8–27.0 million ha are found in Indonesia [1]. This is one of the largest near-surface pools of terrestrial organic carbon [1-4]. Peat swamp forests have a wealth of ecological and hydrological functions such as water retention, flood reduction, protection against seawater intrusion, support of high levels of endemism, and finally as a retreat for endangered species such as the Bornean Orangutan (*Pongo pygmaeus*). Tropical peat typically accumulates in alluvial floodplains where peat swamp forests, over thousands of years, formed convex shaped peat domes up to 20 m thick [5-8]. Persistent anthropogenic impacts by logging and drainage diminish their ability to sequester carbon and conversion to plantations and recurrent uncontrolled fire release huge amounts of carbon dioxide each year [7,9,10]. In particular drainage and forest clearance disturb the hydrological stability [3] and make these otherwise waterlogged ecosystems susceptible to fire [11]. Usually peatland fires are started by farmers to clear land and on a larger scale by private companies as a cheap tool to clear forest before establishing oil palm and pulp wood plantations [12-15]. Fire is particularly acute in Indonesia, where recurrent fires release large amounts of carbon dioxide to the atmosphere [16-18]. This has increased interest in tropical peatlands in the context of global warming [7,9,17,18].

To measure the carbon content it is necessary to determine the carbon density of the peat and the peat volume. Peat thickness is usually measured by using manually operated peat corers at intervals of 500–2,000 m. Since most peatlands in Indonesia are highly inaccessible, very few field measurements have been made to date. To overcome these constraints, Jaenicke *et al.* [10] applied 3D modeling based on the combined analysis of earth observation data and *in situ* peat thickness measurements. They demonstrated that Shuttle Radar Topography Mission (SRTM) data can be used to determine the extent and topography of the dome shaped surface and correlation was obtained between the convex peat dome surface and the depth of the underlying mineral ground, which was determined by manually operated peat corers in the field. These results were then used to calculate the peat volume and carbon store. The main problem of this approach was the determination of the vegetation height growing on peat domes as the SRTM C-band sensor does not penetrate dense and tall vegetation cover straight to the soil surface.

One way to overcome this problem may be the use of aerial Light Detection and Ranging (LiDAR). LiDAR is based on the transmission of laser pulses toward the ground surface and the recording of the return signal. By analyzing the time delay for each pulse reflected back to the sensor, surface elevation can be determined with an accuracy of a few centimeters. The resulting three

dimensional LiDAR point clouds (x, y, and z coordinates) are differentiated into ground points, points reflected from the terrain, and non-ground points mainly reflected from the vegetation in forested regions. The ground points are then used to generate Digital Terrain Models (DTMs). Aerial LiDAR systems (discrete return and full waveform), compared to other remote sensing technologies, have been shown to yield the most accurate estimates for land topography, forest structural properties, and forest Above Ground Biomass (AGB). On the other hand systems operated from airplanes have limitations due to large data volumes and high costs [19].

The GeoScience Laser Altimeter System (GLAS) onboard NASA's Ice, Cloud, and land Elevation Satellite (ICESat) mission is the first spaceborne LiDAR system capable of providing global datasets of the earth's topography [20]. ICESat/GLAS data have been demonstrated to accurately estimate forest structural properties especially well in topographically even areas with uniform forest cover [21-29]. In areas of moderate to high relief the results show lower reliability [25].

Peatlands have an especially smooth topography. The inland peat swamps of Central Kalimantan (Indonesia), for example, have an elevation rise of only about 1 m per km [7,30]. Therefore ICESat/GLAS data might be an adequate tool to measure the topography of the peat soil and the forest AGB. On the other hand, based on the authors' airborne LiDAR data estimates (see Section 2.3.1), the canopy coverage can be higher than 95%, depending on the peat swamp forest subtype and previous logging impacts.

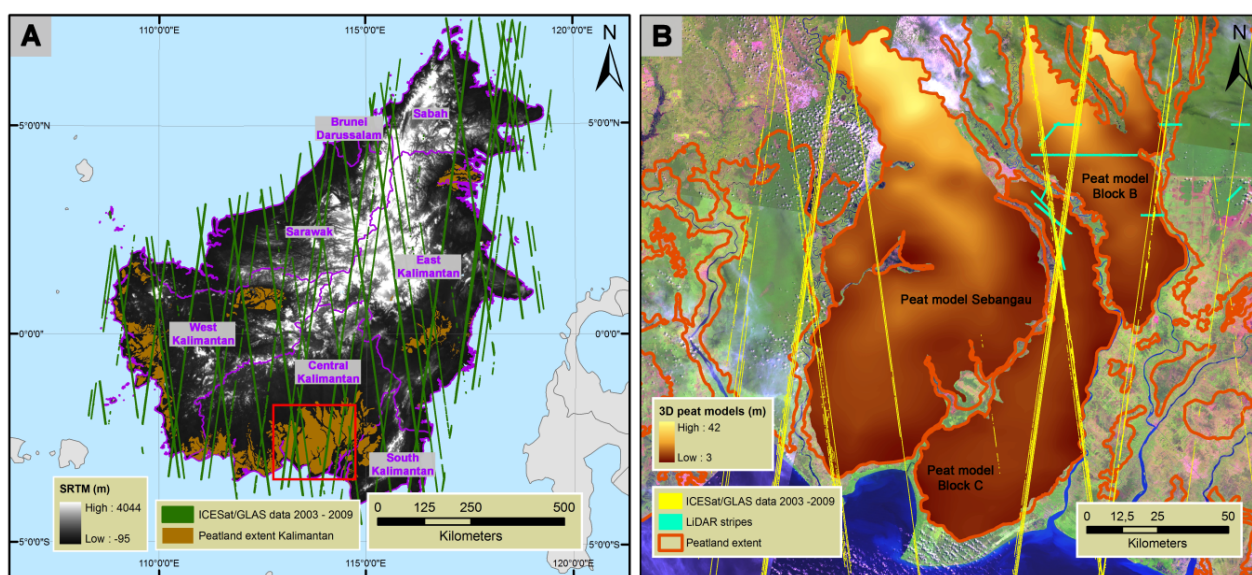
In order to assess the applicability of ICESat/GLAS, the following questions were proposed: (1) Is ICESat/GLAS capable of penetrating the dense peat swamp forest cover and to measure the peat surface topography? (2) How accurate is the SRTM digital elevation model in comparison to ICESat/GLAS measurements on peatlands? (3) How accurate are 3D peatland elevation models derived from SRTM data? (4) How accurate are ICESat/GLAS measurements of peat swamp forest canopy heights compared to airborne LiDAR measurements? (5) Is it possible to derive a peat swamp forest AGB prediction model from ICESat/GLAS data based on airborne LiDAR and forest inventory data?

2. Methodology

2.1. Study Area

Borneo is the third largest island in the world and the largest land mass in the Sundaic area. The island lies in a region (between latitudes 7°N and 4°S) of constant rainfall and high temperatures throughout the year which are ideal conditions for plant growth. Forest types include mangrove forests, peat swamp and freshwater swamp forests, the most extensive extent of heath forests (*kerangas*) in Southeast Asia, lowland dipterocarp forests, ironwood (*ulin*) forests, forests on limestone and ultrabasic soils, hill dipterocarp forests and various montane formations [31]. The major part of Borneo (539,460 km² or 73%) lies within Indonesian territory and is known as Kalimantan; the rest of the island consists of the states of Sarawak and Sabah (together forming East Malaysia) and the independent sultanate of Brunei Darussalam (Figure 1(A)).

Figure 1. Overview of the study area: **(A)**: The island of Borneo and the peatland extent within Kalimantan, Indonesia, derived from maps prepared by Wetland International [32]. Shown are the ICESat/GLAS transects from the years 2003 to 2009, which were used in this study (shots with incorrect elevation flags were filtered out), superimposed on Shuttle Radar Topography Mission (SRTM) data; **(B)**: Location of the investigated 3D peat models and the LiDAR stripes intersecting ICESat/GLAS data within Central Kalimantan superimposed on Landsat TM and ETM+ data (bands 5, 4, 3). Peatland extent (orange outline) and the examined ICESat/GLAS data from the years 2003 to 2009 are also indicated. The red rectangle in (A) shows the location and extent of (B).



The focus of this study is the peatlands of Central Kalimantan. Their extent within Kalimantan was determined from maps prepared by Wetlands International [32] and the authors' Landsat satellite image interpretations (Figure 1(A)). 5.7 million ha or 27.8% of Indonesia's peatland resources are found in Kalimantan [32]. Peat depth varies from very shallow (less than 0.5 m) to very deep peat with up to 12 m [32]. 42% were classified as very deep peat [32]. The three 3D peatland elevation models and airborne LiDAR data were available from other research projects (Figure 1(B)) [10,17]. A detailed description of the methodology on how these 3D peatland elevation models were extracted from SRTM data is given by Jaenicke *et al.* [10]. Within Central Kalimantan all peat swamp forest ecosystems have been severely impacted by extensive logging and drainage for more than two decades [33]. The area also covers the former Mega Rice Project (MRP), an ill-fated transmigrasi resettlement project, initiated in 1995 by the Indonesian government.

2.2. Data

2.2.1. ICESat/GLAS Data

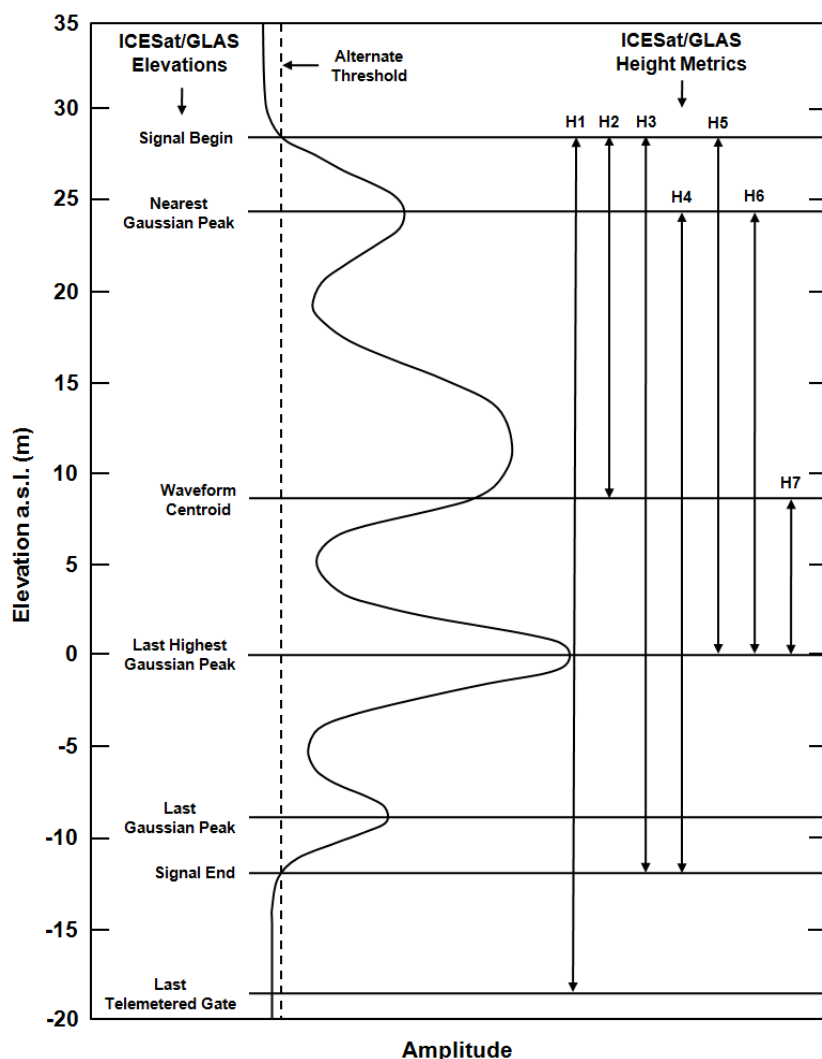
The Ice, Cloud, and land Elevation Satellite (ICESat) has been orbiting the earth since 12 January 2003 at an altitude of 600 km with a 94° inclination and during most of its operating life it has been programmed for a 91-day orbital repeat cycle and was decommissioned from operation on 14 August

2010. The GeoScience Laser Altimeter System (GLAS) onboard ICESat was a full waveform sensor using a 1,064 nm laser operating at 40 Hz. This resulted in a nominal footprint of about 65 m diameter on the earth's surface with each pulse separated by 172 m postings [20]. There were three lasers onboard ICESat of which the first one failed about 38 days into the mission (29 March 2003). The original temporally continuous measurements were replaced by three 33 day operating periods per year, so that the life of the second and third laser could be extended [29]. The laser footprint on the earth's surface actually was in the form of an ellipse and its size varied over time as a function of power output from the laser [25]. As the GLAS sensor recorded the returned energy over time these waveforms represented the vertical distribution of the terrain and vegetation within each footprint. GLAS data have been demonstrated to accurately estimate forest height [26-28] and AGB [22,25]. In this study we used the ICESat/GLAS data product GLA14 Global Land Surface Altimetry Data release version 31 for all acquisition dates from February 2003 to October 2009 for the island of Borneo (Figure 1(A,B)). This data product can be downloaded at The National Snow and Ice Data Center [34]. According to The National Snow and Ice Data Center ICESat/GLAS data release version 31 had an average horizontal geolocation error for all laser campaigns of 0.78 m (± 5.09 m) [35]. For the comparison of the ICESat/GLAS data and SRTM data only ICESat/GLAS data acquired from February 2003 to October 2003 was used, as these are the nearest acquisition dates to the SRTM data (11–22 February 2000), so that potential vegetation cover change could be minimized (see Section 2.2.4). To compare ICESat/GLAS data to the airborne LiDAR data and the 3D peatland elevation models all ICESat/GLAS acquisitions from February 2003 to October 2009 were utilized.

The elevations from the GLA 14 product were obtained by combining Precise Orbit Data (POD) [36], Precise Altitude Data (PAD) [37], and range data. To determine the range data the time stamps between the centroid of the transmitted pulse and the corresponding reference point, mostly the centroid, of the return waveform were compared. Latitude, longitude and footprint elevation were computed [38], after all instrumental, atmospheric, and tidal corrections are applied [39]. The positions of these reference points were then stored as range offsets. The waveforms received by the GLAS sensor were characterized by a single Gaussian peak over oceans, sea ice, and ice sheets, and by multiple peaks over irregular surfaces such as land covered by vegetation. Over vegetated land the GLA14 product extracted information from these complex waveforms by fitting up to six Gaussian distributions to the waveform [25]. From these Gaussian distributions different waveform peaks were derived that describe different features of the vertical vegetation structure and the underlying topography [25]. For tree-covered areas a bimodal GLAS waveform was typical, where topographic relief within a footprint was small compared to vegetation height, which can be used to estimate biophysical parameters. Reflections from the underlying ground, where hit through canopy gaps, and plant surfaces were separated vertically. The height where half of the return energy is above and half below correspond to the centroid of the waveform [40,41]. The distance between the signal beginning and the centroid of the ground return corresponds to the maximum canopy height and can be used as an estimate of AGB [42]. Sometimes the last Gaussian peak is not a good representation of the ground surface, for example when the last peak has a lower amplitude than another peak close to it [22,28]. In this case the higher amplitude peak represents ground surface height [22,28]. The distance between signal begin and signal end corresponds to the total waveform length and also provides information on vegetation height although it is combined with effect of topographic

slope [42]. A simplified overview of the different ICESat/GLAS elevations and height metrics is given in Figure 2. The interpretation of waveforms is significantly more difficult for areas where within-footprint topographic relief is a substantial fraction of the vegetation height, so that the canopy and ground reflections are mixed.

Figure 2. Simplified ICESat/GLAS waveform with four Gaussian peaks. On the left, the location of the different ICESat/GLAS elevations is depicted and, on the right, the varying ICESat/GLAS height metrics derived from them are shown. The Signal Begin and the Signal End of the waveform are defined by the crossing of an Alternate Threshold (dashed line).



2.2.2. Airborne LiDAR Data

Airborne LiDAR data was acquired during a flight campaign conducted between 5 and 10 August 2007 [17]. A Riegl LMS-Q560 Airborne Laser Scanner was mounted to a Bell 206 helicopter. Small-footprint full-waveform LiDAR data was collected from a flight altitude of 500 m above ground over a scan angle of $\pm 30^\circ$ (swath width ± 500 m). The laser sensor had a pulse rate of up to 100,000 pulses per second with a footprint of 0.25 m and a wavelength of 1.5 μm (near infrared). Due

to the accurate time stamping (10^9 samples per second), the three dimensional coordinates of the laser beam reflections (x, y, and z), the intensity, and the pulse width can be extracted by a waveform decomposition, which fits a series of Gaussian pulses to the waveform. This resulted in an average of 1.4 echoes per square meter. The Riegl LMS-Q560 Airborne Laser Scanner system allows height measurements of ± 0.02 m. Single beam measurements have an absolute horizontal accuracy of ± 0.50 m and vertical accuracy of ± 0.15 m Root Mean Square Error (RMSE). 13,626 ha of LiDAR data was available for this study of which 9,702 ha of LiDAR transects were intersected by ICESat/GLAS data (Figure 1(B)).

2.2.3. SRTM Data

The Shuttle Radar Topography Mission (SRTM), a joint mission conducted by the National Aeronautics and Space Administration (NASA) and the National Imagery and Mapping Agency (NIMA), was flown from 11 to 22 February 2000 and collected single-pass radar interferometry data covering 119.51 million km^2 of the earth's surface including over 99.9% of the land area between 60°N and 56°S latitude. The C-band InSAR acquired data in 225 km swaths and was provided by the Jet Propulsion Laboratory (JPL). For Southeast Asia digital elevation models with a pixel spacing of three arcseconds (about 90 m) were produced. The absolute horizontal and vertical accuracy of the data are better than 20 and 16 m respectively [43].

2.2.4. MODIS Data

To determine potential vegetation cover change between the acquisition of the SRTM data (11–22 February 2000) and the ICESat/GLAS data (February 2003 to October 2003) the area proportional estimate of woody vegetation, provided in the 500 m resolution Vegetation Continuous Fields (VCF) product from the Moderate Resolution Imaging Spectroradiometer (MODIS) was used, which is referred to as the percent tree cover layer [44]. Hansen *et al.* [44] used global training data derived from high resolution imagery to extract VCF woody vegetation, herbaceous vegetation, and bare cover estimates from cloud-corrected, monthly composites of MODIS surface reflectance.

2.2.5. Field Inventory Data

Field inventory data in Central Kalimantan was collected from May to August 2008. 9 Clusters each with four sample plots were selected depending on representativeness of forest, sub forest and land use type, and accessibility. The cluster positions were set in advance to assure that they lie within the swath of the aerial LiDAR data set. A GPS device (Garmin GPS map60CSx, accuracy of 3 to 10 m) was used to locate the position of the clusters, as well as to mark the center of each sample plot. The four sample plots of one cluster build the corners of a 50×50 m square. In each sample plot trees were measured using the nested plot method which is based on circular fixed-area plots [45]. Three nests of circular shape with radii of 4, 14 and 20 m were used. Trees with a Diameter at Breast Height (DBH) smaller than 7 cm were excluded. In each nest, trees of a certain DBH range were measured: 7 to 20 cm (4 m radius), 20 to 50 cm (14 m radius), and greater than 50 cm (20 m radius). For each tree following parameters were recorded: local species name, DBH in cm, and tree height in m.

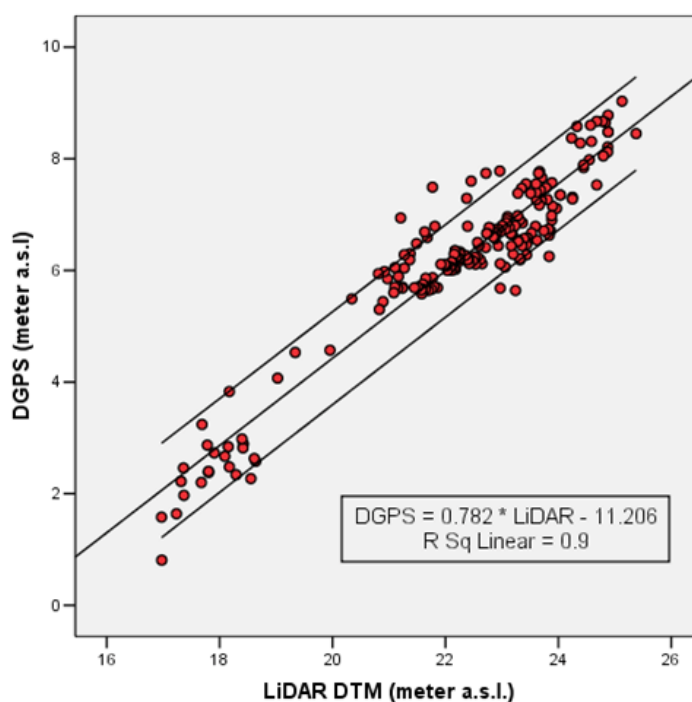
Local names were translated to corresponding Latin names through information provided by the experts of a local herbarium at the Centre for International Co-operation in Management of Tropical Peatland (CIMTROP) in Palangka Raya and tropical timber databases provided by Chudnoff [46] and the World Agroforestry Centre [47]. Species specific wood densities were also derived from these databases as well as from IPCC [48]. Some local names could not be translated and some trees could not be identified in the field. In these cases an average specific wood density for Asian tropical trees, 0.57 Mg m^{-3} , was applied [49]. AGB was calculated using an allometric model of Chave *et al.* [50] for moist tropical forests which includes DBH and wood density but not tree height. We decided to use a model which excludes tree height as accurate tree height measurements in this tropical ecosystem are almost impossible due to the dense and tall forest canopy. 36 sample plots, located in peat swamp forest, were used to compare AGB calculated in the field to airborne LiDAR 3D point cloud height statistics.

2.3. Data Analysis

2.3.1. Airborne LiDAR Data Processing and Correlation with Field Inventory Data

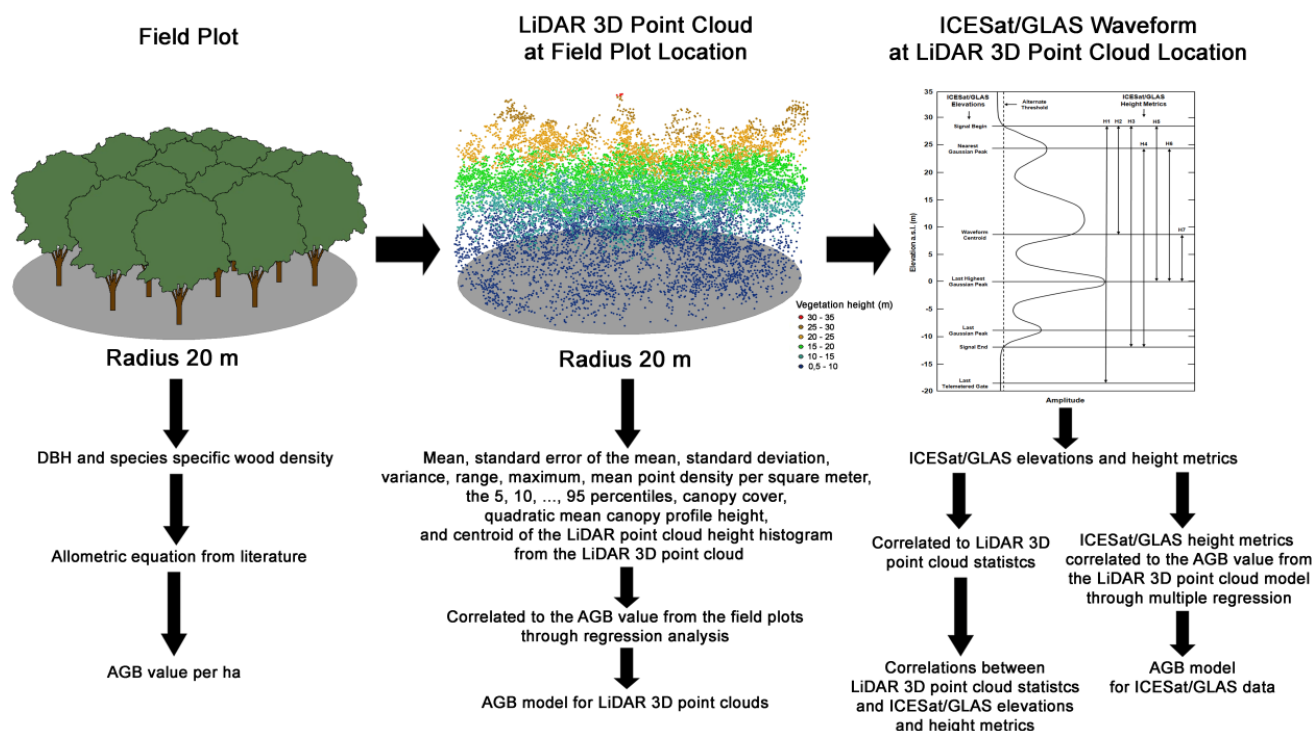
A filtering algorithm based on Kraus and Pfeifer [51] was applied to differentiate between ground and vegetation points within the airborne LiDAR 3D point clouds. Every track was examined further in small subsets to validate the results and manually delete outliers. Digital Terrain Models (DTMs) were then generated by interpolating the filtered ground points. Kriging interpolation was applied (cell size 1 m) as it showed the best results.

Figure 3. Correlation of the airborne LiDAR derived DTMs and the Differential Global Positions System (DGPS) points collected in the field ($R^2 = 0.9$, $n = 201$). Also shown are the 95% confidence intervals.



In order to assure the quality of the generated LiDAR DTMs, 201 field points measured with a Differential Global Positioning System (DGPS) were correlated to the interpolated LiDAR DTMs. A high correlation coefficient ($R^2 = 0.9$) between both data sets was observed (Figure 3). This proves the quality of the LiDAR derived DTMs. The altitude differences observed are due to the use of different height reference systems. Also small deviations are expected, since the LiDAR point clouds are from August 2007 and the DGPS measurements from August 2010, and this time shift can lead to discrepancies, mainly near to canals, due to new fires and peat subsidence.

Figure 4. Overview of the methodology to derive Above Ground Biomass (AGB) values from the field plots (left), the development of AGB models by correlating AGB from the field to airborne LiDAR 3D point clouds statistics (middle), and the correlation of ICESat/GLAS elevations and height metrics to LiDAR 3D point cloud statistics and the development of a AGB model by correlating AGB results from the airborne LiDAR AGB model to ICESat/GLAS height metrics (right).



The LiDAR 3D point cloud statistics within a defined polygon were correlated to the corresponding ground-based AGB value. Linear and multiple linear regression analysis were applied to identify the best AGB estimation model. 36 sample plot centers were expanded by a circle with a radius of 20 m. These areas were used to clip the LiDAR 3D point clouds. The height above the terrain (absolute vegetation heights) for each point within the cloud was determined by subtracting the corresponding pixel value of the DTM. Only points with a value higher than 0.5 m were included in the analysis. LiDAR point height distributions of each sample plot were analyzed statistically and following metrics were derived and used as predictors: mean, Standard Error of the Mean (SEM), standard deviation, variance, range, maximum, mean point density per square meter, and the quantiles corresponding to the 5, 10, ..., 95 percentiles of the distributions. As further potential predictors

Canopy Cover (CC), the Quadratic Mean Canopy profile Height (QMCH) [52] and the centroid of the LiDAR point cloud height histogram (CL) were determined. For every pixel of a certain size (5 m), CC was calculated by dividing the number of points above a certain height threshold (10 m) by the number of points below the threshold. A schematic overview of this approach is shown in Figure 4. For final model validation, the coefficient of determination (R^2), the corrected coefficient of determination (R^2_{corr}), and the Standard Error of the Estimate (SEE) were used.

2.3.2. ICESat/GLAS Data Processing and Analysis

The original GLA14 data product was converted to the ESRI point Shape file format using an in house Java script. GLA14 data contains elevations with respect to the TOPEX/Poseidon-Jason Ellipsoid [20]. For the reason of comparison GLA14 data was converted to the WGS84 ellipsoid and orthometric elevations were obtained by applying the EGM96 geoid. In ArcGis 9.3 the elliptical footprints for the individual shots were extracted. Only footprints located completely on peatland were selected [32] (Figure 1(A)).

The SRTM data, three 3D peatland elevation models in Central Kalimantan (Figure 1(B)), and MODIS VCF product for the years 2000 and 2003 were resampled to 5 m with the nearest neighbor interpolation method. Additionally the slope in degrees was calculated from the SRTM data by using a 3×3 moving window which then was also resampled to 5 m. From these layers for each ICESat/GLAS footprint zonal statistics were extracted.

Furthermore a number of different ICESat/GLAS elevations and height metrics were calculated (Figure 2).

A range of different filters were generated. To avoid terrain slope and heterogeneous effects the SLOPE filter indicates whether the slope, derived from the interpolated SRTM slope layer, in a footprint is less than 10 degrees or not. The SATURATION filter shows whether an ICESat/GLAS waveform suffers from saturation. To define this filter the *i_satCorrFlg* flag from the GLA14 records was utilized. If there is a thin cloud cover ICESat/GLAS data is returned from the earth's surface, but a thick cloud layer may prevent the laser pulse from reaching the ground and either no return is detected or the return is from the cloud top [53]. To prevent this outlier occurrence the OUTLIER filter was implemented. This filter indicates whether the ICESat/GLAS elevation is more than 100 m above the SRTM elevation as these records are associated with laser returns from cloud tops [53]. Additionally the ATMOSPHERE filter was established, defined by the *i_FRir_qaFlag* flag of the GLA14 data product, which indicates the presence of clouds. All waveforms ≤ 60 m are indicated by the WAVEFORM EXTENT filter. The ELEVATION filter indicates whether the elevation information of a footprint can be considered as valid and is defined by the *i_ElvuseFlg* flag. With the help of the GLA14 *i_rng_UQF* flag the RANGE filter is determined which indicates the quality of the range increments. The filters VCF CHANGE 0% to VCF CHANGE 25% show the woody vegetation change in percent between the years 2000 and 2003 defined by the MODIS VCF product. Through visual comparison of the ICESat/GLAS footprints and Landsat imagery the vegetation change between the acquisition of the ICESat/GLAS data and the acquisition of the airborne LiDAR data was assessed and the footprints were classified into 8 vegetation change classes (no change, forest-degraded forest, forest-deforested area, degraded forest-deforested area, degraded forest-forest,

deforested area–forest, deforested area–degraded forest, water). This VEGETATION CHANGE filter could then be used to exclude ICESat/GLAS footprints with a vegetation change from the statistical comparison.

2.3.3. Comparison ICESat/GLAS and Airborne LiDAR Data

ICESat/GLAS footprints located completely within airborne LiDAR point clouds were selected. For these footprints, on average about 65 m in diameter, different statistics from the airborne LiDAR point clouds and the DTMs were calculated and then correlated to the corresponding ICESat/GLAS elevations. Statistics included: minimum, maximum, mean of the z values from the airborne LiDAR points and DTMs within the ICESat/GLAS footprints. Furthermore different statistics from the normalized airborne LiDAR point clouds (z values of the airborne LiDAR points minus the corresponding DTM values) were correlated to ICESat/GLAS height metrics H1–H7 (Figure 2). Statistics included: minimum, maximum, mean, and the 5, 10, ..., 95 percentiles. Additionally the Quadratic Mean Canopy profile Height (QMCH) and the centroid of the LiDAR point cloud height histogram (CL) were compared to these ICESat/GLAS height metrics. A schematic overview of this approach is shown in Figure 4.

2.3.4. Development of Above Ground Biomass Prediction Models from ICESat/GLAS Data

Again ICESat/GLAS footprints located completely within airborne LiDAR point clouds were selected. For these footprints the airborne LiDAR point statistics of the 20 m circular buffers at footprint center (representing the 20 m field plots with a size of 0.13 ha) were used to calculate AGB derived from the airborne LiDAR regression models (Section 2.3.1, Figure 4). These AGB values at ICESat/GLAS footprint location were then correlated to different ICESat/GLAS height metrics. Multiple linear regression analysis was applied to create ICESat/GLAS AGB estimation models.

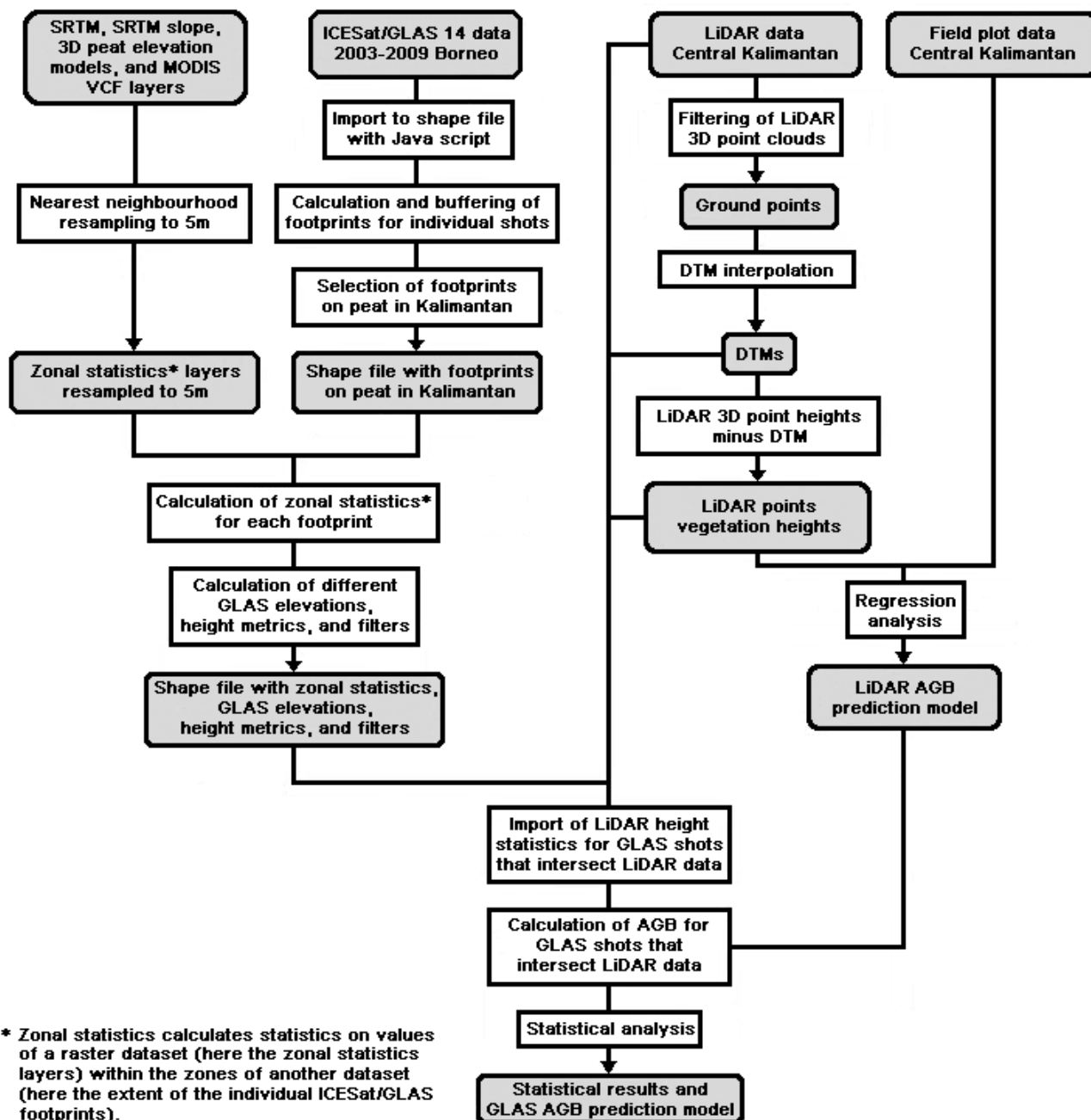
Following ICESat/GLAS height metrics were used as predictors: last telemetered gate–signal begin (H1), waveform centroid–signal begin (H2), signal end–signal begin (H3), signal end–nearest Gaussian peak (H4), last highest Gaussian peak–signal begin (H5), last highest Gaussian peak–nearest Gaussian peak (H6), and last highest Gaussian peak–waveform centroid (H7) (Figure 2).

Stepwise and backward selection was performed to determine which independent variables should be included in the final models. For final model validation, the coefficient of determination (R^2), the corrected coefficient of determination (R^2_{corr}), and the Standard Error of the Estimate (SEE) were used. Figure 4 shows a simplified overview of this approach.

2.3.5. Conceptual Overview

Figure 5 gives a conceptual overview of the methodology described above.

Figure 5. Conceptual overview of the methodology used in this study.



3. Results

3.1. Comparison ICESat/GLAS, SRTM Data, and SRTM 3D Peatland Elevation Models

The ICESat/GLAS data is referenced to a consistent geodetic reference frame, so that its horizontal and vertical geolocation accuracy and its ability to resolve the height distribution of elevations within the laser footprint, provides a set of accurate control points which can be used to investigate the vertical accuracy of the SRTM digital elevation model [53]. ICESat/GLAS’s capability to measure the vertical distribution of forests and the underlying surface is useful to assess especially the SRTM C-band microwave penetration depth into these forested areas [53]. First we established correlations between SRTM mean elevation at footprint location and ICESat/GLAS elevations of signal begin,

waveform centroid, and signal end on peatlands for the whole of Kalimantan. In 2003 9,849 ICESat/GLAS footprints were recorded on peatlands in Kalimantan. This ICESat/GLAS data were quality filtered to incorporate valid and usable footprints for further analyses. Only footprints with a slope of less than 10 degrees and with an ICESat/GLAS elevation not more than 100 m above the SRTM elevation, indicated by the SLOPE and OUTLIER filters respectively, were used. Waveforms that suffer from saturation or that indicate the presence of clouds were excluded using the SATURATION and ATMOSPHERE filters. Furthermore footprints with a waveform >60 m, without valid elevation information, and without sufficient quality of the range increments, indicated by the WAVEFORM EXTENT, the ELEVATION, and the RANGE filters respectively, were also excluded. Finally for the statistical analysis we only used footprints that show a vegetation cover change of less than 15% between the years 2000 and 2003 (derived from the MODIS VCF product and represented by the VCF CHANGE 15% filter). The ICESat/GLAS elevations of the signal begin, waveform centroid, and the signal end of the remaining 4,186 shots were correlated to the corresponding mean SRTM elevation. The R^2 values are 0.88, 0.92, and 0.60 respectively, where waveform centroid shows the highest correlation. Figure 6 displays the results of this correlation in three scatter plots. The mean ICESat/GLAS and SRTM elevation differences are 8.7 m (± 6.1 m) for signal begin, -4.9 m (± 3.8 m) for waveform centroid, and -16.1 m (± 8.4 m) for signal end. This result also indicates that the SRTM C-band phase is not reflected by the top of the peat swamp forest canopy but somewhere within the 3D forest structure. Figure 7(B) suggests that on average the C-band penetrates approximately 10–15 m into the forest cover.

Figure 6. Scatter plots displaying the correlation between ICESat/GLAS signal begin, waveform centroid, and signal end elevations a.s.l. (m) to the mean elevation a.s.l. (m) of the corresponding SRTM data. All ICESat/GLAS footprints are from the year 2003 and located on peatlands. The elevation of the waveform centroid with a coefficient of determination (R^2) of 0.92 shows the highest correlation to the SRTM data.

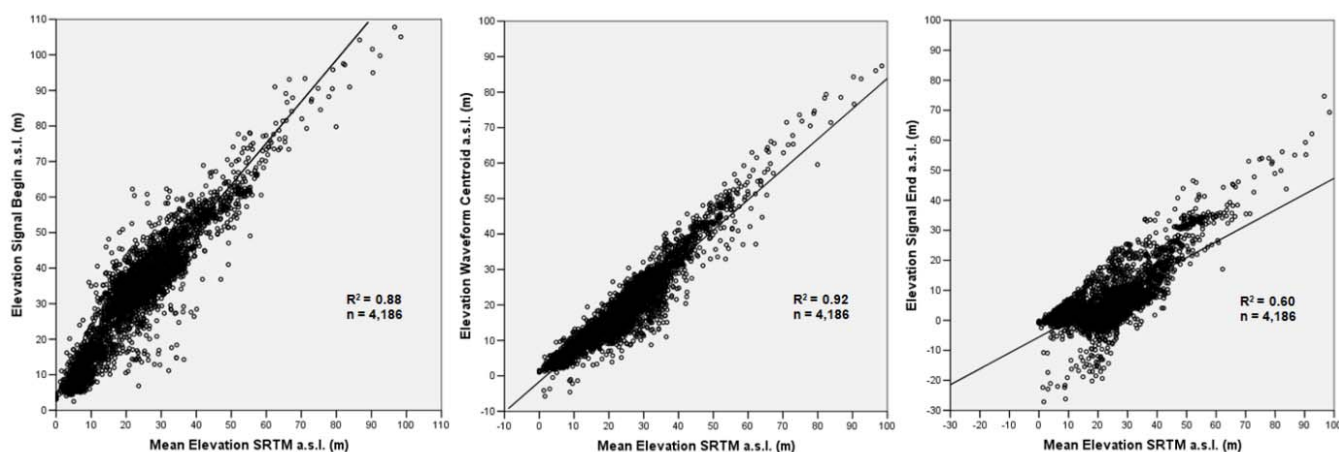
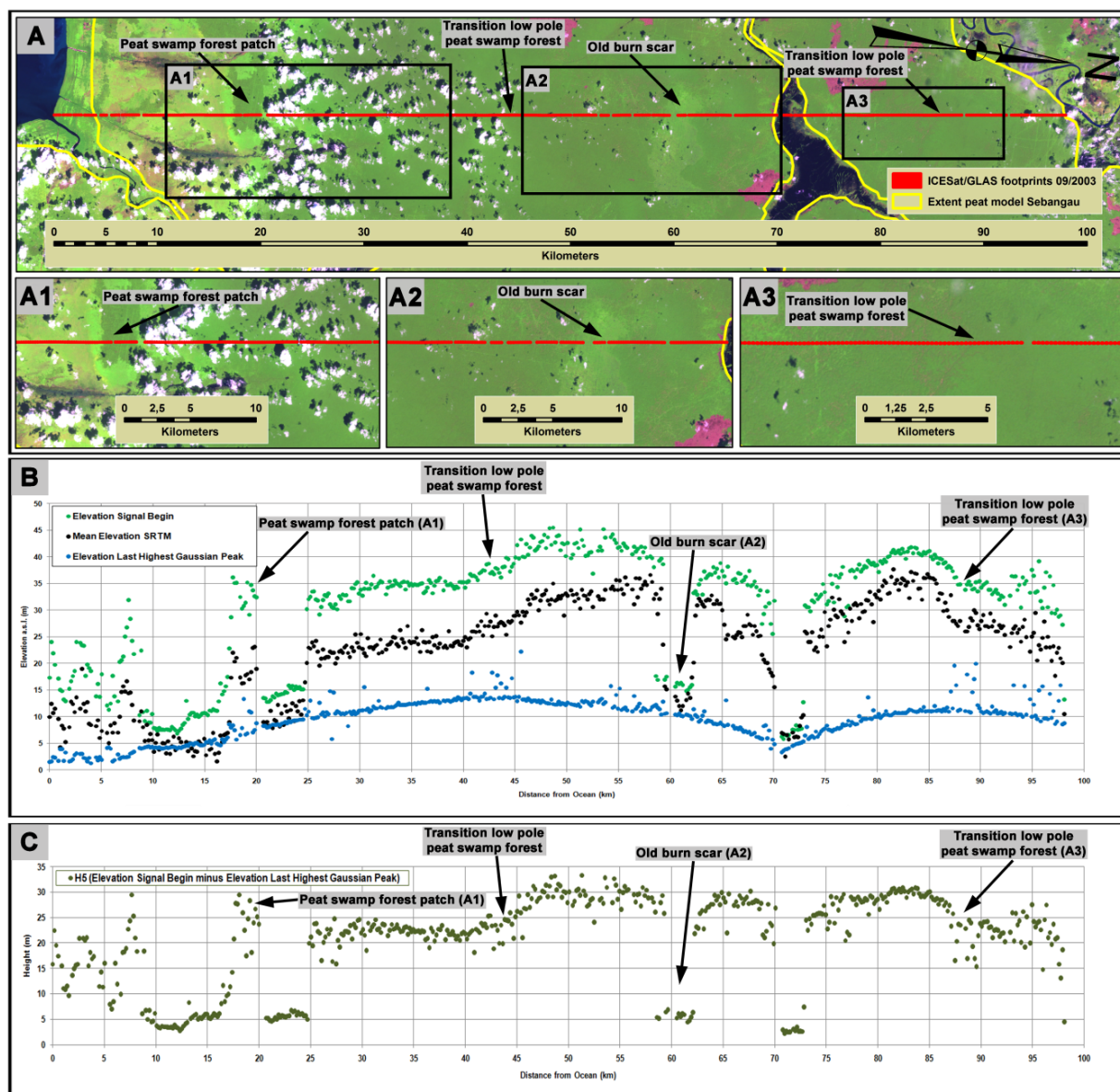


Figure 7. ICESat/GLAS transect covering the Sebangau peatland area from south to north. The transect of 98 km length starts at the ocean in the south then transects heavily degraded forest, logged peat swamp forest, an old burn scar, and further north a lake, and peat swamp forest again. (A): ICESat/GLAS transect superimposed on a Landsat ETM+ image (22-05-2003, bands 5, 4, 3). Bright green represents degraded forest, dark green peat swamp forest. A1–A3: Three enlarged areas within this ICESat/GLAS footprint transect. The locations of these areas are indicated by the three black rectangles in A; (B): Elevation profile of the ICESat/GLAS transect. Shown are the ICESat/GLAS elevations for the forest canopy (green) and the peat surface (blue). Note the curvature of the peat dome. Also displayed is the mean elevation at footprint location from the SRTM data (black). The locations of a peat swamp forest fragment, two low pole peat swamp forest transition zones, and an old burn scar are indicated by black arrows; (C): Measurement of absolute vegetation height by subtracting ICESat/GLAS peat surface elevation from ICESat/GLAS forest canopy signals (ICESat/GLAS height metric H5).



Based on the results above, it is reasonable to use ICESat/GLAS data as a tool to validate 3D peatland elevation models which were derived from SRTM data. 14,312 footprints acquired between 2003 and 2009 were located on the three investigated 3D peatland elevation models (see location in Figure 1). For these footprints we applied the same filters as described above with exception of the VCF CHANGE 15% filter as this was not necessary. After filtering 4,045 footprints remained, of which 1,116 were located on the peat model Sebangau, 1,244 on the peat model Block B, and 1,685 on the peat model Block C. As the elevation from the last highest Gaussian peak is known to correspond best with the actual surface elevation [22,28] this parameter was correlated to the mean elevation of the three 3D peatland elevation models. The R^2 value for this correlation is 0.90. Although some of the elevations of the 3D peatland elevation models differ from the corresponding elevations of the last highest Gaussian peak the mean difference between the two elevation parameters was only -1.0 m (± 3.2 m).

Furthermore we investigated specific ICESat/GLAS footprint transects in more detail for several well investigated peat domes in Central Kalimantan. Figure 7 shows one transect that extends 98 km from south to north over the Sebangau peat dome. The transect starts at the coastline in the south and first covers heavily degraded peat swamp forest with some remaining tall forest fragments, then more or less disturbed tall peat swamp forest, an old burn scar, a lake with adjacent wetland scrubs and further north again peat swamp forest which has been logged 20 years ago. From the elevation of the ICESat/GLAS signal begin, which corresponds to the top of the forest canopy, these different vegetation types are clearly discernible (Figure 7(B)). Also apparent is a variation in the forest canopy height of the peat swamp forest which is related to different subtypes of peat swamp forests (low pole, medium, and tall). This is clearly visible in Figure 7(B,C) at km 42 and 87. In Figure 7(C) the elevation of the last highest Gaussian peak is subtracted from the elevation of the signal begin (ICESat/GLAS height metric H5) and so showing the absolute vegetation height. Also shown in Figure 7(B) is the corresponding mean SRTM elevation. The penetration depth of the SRTM C-band phase center into the forest canopy can be assessed. On deforested sites the SRTM C-band phase center and the last highest Gaussian peak match to each other and represent the surface elevation. The blue line in Figure 7(B) indicates the peat surface topography across a vast distance with high accuracy using ICESat/GLAS. Over a distance of 30 km the peat surface increases from 5 to 15 m and forms a convex shape which is typical for peat swamp ecosystems.

3.2. Comparison ICESat/GLAS and Airborne LiDAR Data

In order to compare ICESat/GLAS derived elevations with those of airborne LiDAR measurements ICESat/GLAS footprints located completely within airborne LiDAR point clouds were selected. After filtering 104 valid footprints remained.

We correlated the minimum, maximum, and mean z values from the airborne LiDAR points and DTMs to the signal begin, nearest Gaussian peak, waveform centroid, last highest Gaussian peak, last Gaussian peak, and signal end from the ICESat/GLAS data. The results of these correlations are displayed in Table 1. The highest correlation, with a R^2 value of 0.91, was observed when comparing the mean z value of the airborne LiDAR points to the waveform centroid of the ICESat/GLAS data. Also high correlations are evident for the comparison of the maximum and mean z values of the

LiDAR points to the signal begin of the ICESat/GLAS data and the maximum z values of the airborne LiDAR points to the waveform centroid of the ICESat/GLAS data (Table 1). The mean elevation difference between these two data sets was -0.5 m (± 1.9 m) for waveform centroid and the mean z value, 2.3 m (± 3.3 m) for the last highest Gaussian Peak and the minimum z value, and 3.2 m (± 3.2 m) for signal begin and the maximum z value.

Table 1. Coefficients of determination (R^2) for the correlation of the minimum, maximum, and mean of the z values from the airborne LiDAR points and DTMs with different ICESat/GLAS elevation parameters. Where n is the number of ICESat/GLAS footprints used for the comparison. The highest coefficients of determination (R^2) are bold.

| Airborne LiDAR statistics | ICESat/GLAS elevations | | | | | | |
|---------------------------|------------------------|--------------|-----------------------|-------------------|----------------------------|--------------------|------------|
| | n | Signal begin | Nearest Gaussian peak | Waveform centroid | Last highest Gaussian peak | Last Gaussian peak | Signal end |
| Minimum z | 103 ^a | 0.50 | 0.48 | 0.61 | 0.63 | 0.68 | 0.66 |
| Maximum z | 103 ^b | 0.86 | 0.76 | 0.81 | 0.48 | 0.43 | 0.42 |
| Mean z | 104 | 0.84 | 0.77 | 0.91 | 0.60 | 0.60 | 0.59 |
| Minimum DTM | 104 | 0.57 | 0.54 | 0.67 | 0.63 | 0.71 | 0.67 |
| Maximum DTM | 104 | 0.57 | 0.54 | 0.67 | 0.62 | 0.70 | 0.67 |
| Mean DTM | 104 | 0.57 | 0.54 | 0.67 | 0.62 | 0.71 | 0.67 |

^a Footprints with a minimum z value <0 m were considered as outliers and removed; ^b Footprints with a maximum z value >100 m were considered as outliers and removed.

Statistics from the normalized airborne LiDAR point clouds (z values of the airborne LiDAR points minus the corresponding DTM values) were then compared to ICESat/GLAS height metrics H1–H7 (Figure 2). Statistics included: minimum, maximum, mean, the 5, 10, ..., 95 percentiles, Quadratic Mean Canopy profile Height (QMCH), and the centroid of the LiDAR point cloud height histogram (CL). The results are shown in Table 2. The highest R^2 values were found when correlating percentile 95 with the ICESat/GLAS height metrics with exception of H7 where 80% had the highest R^2 . The overall highest correlation was between percentile 95 and ICESat/GLAS height metric H3.

Table 2. Coefficients of determination (R^2) for minimum, maximum, mean, the 5, 10, ..., 95%, Quadratic Mean Canopy profile Height (QMCH), and the centroid of the LiDAR point cloud height histogram (CL) from the normalized airborne LiDAR point clouds (z values of the airborne LiDAR points minus the corresponding DTM values) correlated to ICESat/GLAS height metrics H1–H7 (Figure 2). Where n is the number of ICESat/GLAS footprints used for the comparison. The highest coefficients of determination (R^2) are bold.

| Airborne LiDAR statistics | ICESat/GLAS heights metrics | | | | | | | |
|---------------------------|-----------------------------|------|------|------|------|------|------|------|
| | n | H1 | H2 | H3 | H4 | H5 | H6 | H7 |
| Minimum | 102 ^a | 0.01 | 0.00 | 0.00 | 0.01 | 0.00 | 0.00 | 0.00 |
| Maximum | 103 ^b | 0.40 | 0.46 | 0.54 | 0.42 | 0.49 | 0.33 | 0.28 |
| Mean | 104 | 0.26 | 0.22 | 0.36 | 0.30 | 0.34 | 0.25 | 0.29 |

Table 2. Cont.

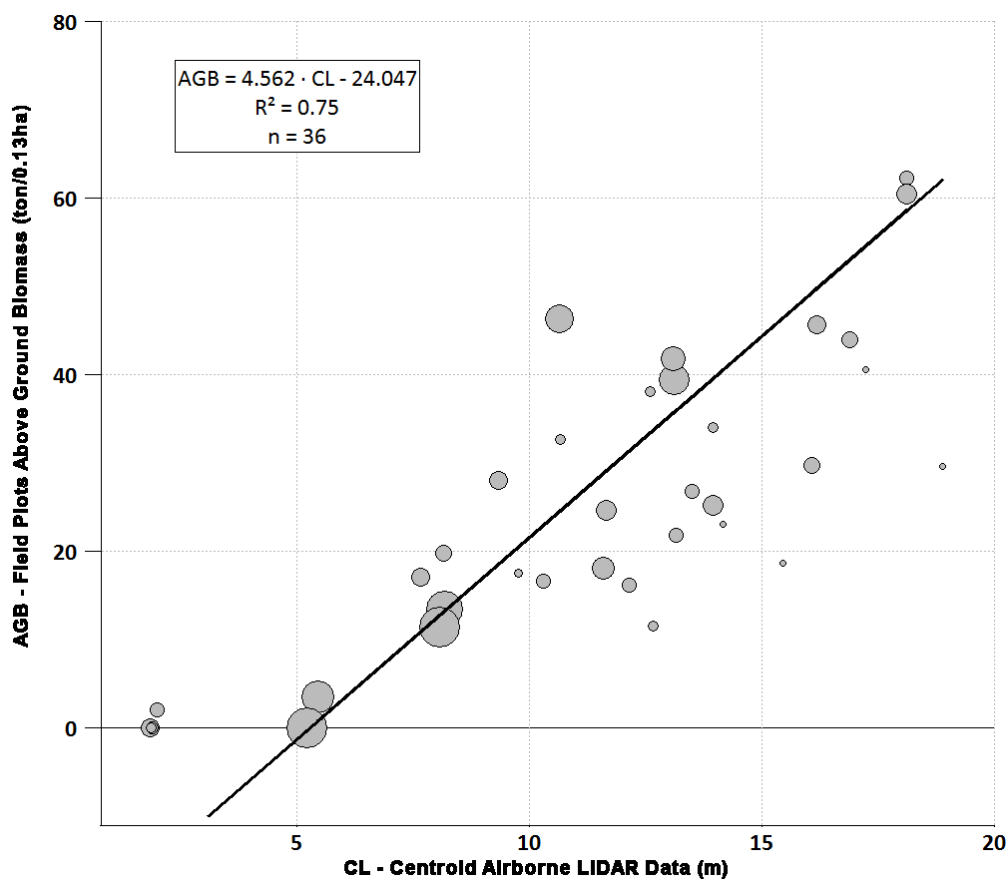
| Airborne LiDAR statistics | ICESat/GLAS heights metrics | | | | | | | |
|------------------------------|-----------------------------|-------------|-------------|-------------|-------------|-------------|-------------|-------------|
| | n | H1 | H2 | H3 | H4 | H5 | H6 | H7 |
| 5% | 104 | 0.00 | 0.00 | 0.00 | 0.00 | 0.00 | 0.01 | 0.01 |
| 10% | 104 | 0.00 | 0.01 | 0.01 | 0.00 | 0.00 | 0.00 | 0.00 |
| 15% | 104 | 0.00 | 0.01 | 0.02 | 0.01 | 0.00 | 0.00 | 0.00 |
| 20% | 104 | 0.00 | 0.01 | 0.03 | 0.02 | 0.01 | 0.01 | 0.01 |
| 25% | 104 | 0.01 | 0.02 | 0.05 | 0.04 | 0.04 | 0.02 | 0.04 |
| 30% | 104 | 0.03 | 0.03 | 0.09 | 0.07 | 0.07 | 0.04 | 0.08 |
| 35% | 104 | 0.09 | 0.06 | 0.16 | 0.13 | 0.15 | 0.10 | 0.17 |
| 40% | 104 | 0.14 | 0.09 | 0.22 | 0.17 | 0.22 | 0.15 | 0.25 |
| 45% | 104 | 0.18 | 0.11 | 0.25 | 0.19 | 0.24 | 0.16 | 0.26 |
| 50% | 104 | 0.21 | 0.13 | 0.28 | 0.22 | 0.28 | 0.18 | 0.29 |
| 55% | 104 | 0.26 | 0.17 | 0.34 | 0.26 | 0.34 | 0.23 | 0.34 |
| 60% | 104 | 0.29 | 0.20 | 0.38 | 0.30 | 0.38 | 0.26 | 0.36 |
| 65% | 104 | 0.33 | 0.24 | 0.43 | 0.36 | 0.42 | 0.31 | 0.39 |
| 70% | 104 | 0.37 | 0.29 | 0.48 | 0.40 | 0.47 | 0.36 | 0.41 |
| 75% | 104 | 0.40 | 0.33 | 0.51 | 0.44 | 0.51 | 0.40 | 0.42 |
| 80% | 104 | 0.42 | 0.36 | 0.53 | 0.47 | 0.53 | 0.43 | 0.43 |
| 85% | 104 | 0.43 | 0.39 | 0.53 | 0.48 | 0.54 | 0.44 | 0.41 |
| 90% | 104 | 0.42 | 0.41 | 0.53 | 0.49 | 0.53 | 0.44 | 0.38 |
| 95% | 104 | 0.45 | 0.47 | 0.57 | 0.50 | 0.56 | 0.45 | 0.37 |
| 100% | 103 ^b | 0.40 | 0.46 | 0.54 | 0.42 | 0.49 | 0.33 | 0.28 |
| QMCH | 102 ^c | 0.27 | 0.23 | 0.40 | 0.35 | 0.39 | 0.34 | 0.31 |
| CL | 104 | 0.28 | 0.21 | 0.38 | 0.32 | 0.37 | 0.35 | 0.28 |

^a Footprints with a minimum z value >5 m were considered as outliers and removed; ^b Footprints with a maximum z value >100 m were considered as outliers and removed; ^c Footprints where QMCH could not be calculated were excluded

3.3. Above Ground Biomass Prediction Models from Airborne LiDAR Data and ICESat/GLAS Data

To derive an AGB prediction model from ICESat/GLAS we used the model derived from airborne LiDAR and forest inventory data. In a first step 36 forest sample plots were used to correlate AGB values calculated in the field to airborne LiDAR 3D point clouds. The best overall predictor of AGB was the centroid of the airborne LiDAR point cloud height histogram (CL). The model could further be enhanced through incorporating the average LiDAR point density per square meter per sample plot of all LiDAR points. Sample plots with a higher average LiDAR point density per square meter were weighted higher during the computation of the final model (Figure 8). The average LiDAR point densities per square meter for these 36 sample plots were between 0.2 and 3.6. The R^2 value of this model is 0.75, the corrected coefficient of determination (R^2_{corr}) is 0.73, and the Standard Error of the Estimate (SEE) is 2.66 ton 0.13 ha⁻¹.

Figure 8. Scatter plot displaying the correlation between the Above Ground Biomass (AGB), calculated from field plots, to the centroid of the airborne LiDAR point cloud height histogram (CL). The sizes of the circles represent the average LiDAR point density per square meter (small = lower average LiDAR point density per square meter; big = higher average LiDAR point density per square meter).



To analyze biomass estimates from ICESat/GLAS we selected only footprints, where the 20 m radius circular buffers at footprint center (representing the field plot size of 0.13 ha) were completely located within the airborne LiDAR point clouds. After filtering 104 valid footprints remained.

The centroid of the airborne LiDAR point cloud height histogram (CL) at these footprints was correlated to the ICESat/GLAS height metrics H1–H7 (Figure 2) depending on the average LiDAR point density per square meter per 20 m radius circular buffer. The corresponding R^2 values are shown in Table 3. The highest R^2 values were found for H5 with average LiDAR point densities per square meter ≥ 0.7 and ≥ 0.8 .

Stepwise and backward multiple regression approaches, incorporating all 7 ICESat/GLAS height metrics (H1–H7), were applied to determine which independent variables should be included in the final models. The highest R^2 value of 0.61 ($n = 35$) was reached through a backward multiple regression approach with H1, H2, H4, H6, and H7 as independent variables and where the average LiDAR point density per square meter was ≥ 0.8 points. The corrected coefficient of determination (R^2_{corr}) was 0.54 and the Standard Error of the Estimate (SEE) 9.76 ton 0.13 ha⁻¹. The mean difference between the ICESat/GLAS AGB estimation and the airborne LiDAR AGB estimation was -2.62 ton 0.13 ha⁻¹ (± 10.78 ton 0.13 ha⁻¹, $n = 104$).

Table 3. Coefficients of determination (R^2) for the ICESat/GLAS height metrics (H1–H7; Figure 2) correlated to the centroid of the airborne LiDAR point cloud height histogram (CL) at the 20 m radius circular buffers at footprint center (representing the field plot size) dependent on the average LiDAR point density per square meter. Where n is the number of ICESat/GLAS footprints used for the comparison. The highest coefficients of determination (R^2) are bold.

| Average LiDAR point density per square m | n | ICESat/GLAS height metrics | | | | | | |
|---|-----|----------------------------|-------------|-------------|-------------|-------------|-------------|-------------|
| | | H1 | H2 | H3 | H4 | H5 | H6 | H7 |
| all | 104 | 0.32 | 0.25 | 0.43 | 0.37 | 0.44 | 0.33 | 0.40 |
| ≥0.1 | 93 | 0.40 | 0.31 | 0.51 | 0.43 | 0.52 | 0.40 | 0.46 |
| ≥0.2 | 72 | 0.45 | 0.34 | 0.54 | 0.49 | 0.59 | 0.53 | 0.56 |
| ≥0.3 | 54 | 0.55 | 0.45 | 0.63 | 0.60 | 0.67 | 0.62 | 0.63 |
| ≥0.4 | 47 | 0.65 | 0.55 | 0.69 | 0.66 | 0.70 | 0.63 | 0.67 |
| ≥0.5 | 46 | 0.68 | 0.57 | 0.73 | 0.68 | 0.75 | 0.65 | 0.71 |
| ≥0.6 | 43 | 0.70 | 0.60 | 0.74 | 0.69 | 0.75 | 0.67 | 0.70 |
| ≥0.7 | 41 | 0.72 | 0.62 | 0.75 | 0.71 | 0.77 | 0.70 | 0.70 |
| ≥0.8 | 39 | 0.72 | 0.62 | 0.74 | 0.71 | 0.77 | 0.71 | 0.72 |
| ≥0.9 | 35 | 0.70 | 0.61 | 0.75 | 0.73 | 0.76 | 0.71 | 0.70 |
| ≥1 | 32 | 0.73 | 0.63 | 0.76 | 0.74 | 0.76 | 0.70 | 0.68 |

4. Discussion and Conclusions

Since most peatlands in Indonesia are highly inaccessible, very few field measurements have been made to date to assess these carbon pools. Especially the potential spatial variation is unknown because up-to-date no systematic large scale sampling has been undertaken. ICESat/GLAS data have been demonstrated to accurately estimate forest structural properties especially well in topographically even areas [21–29]. As peatlands have an especially smooth topography [7,30] we assessed the applicability of ICESat/GLAS data to measure peatland topography, peat swamp forest vertical structure, and peat swamp forest AGB in Central Kalimantan, Indonesia. ICESat/GLAS data was compared to different other data (SRTM data, 3D peatland elevation models derived from SRTM data, and airborne LiDAR data).

Jaenicke *et al.* [10] demonstrated that SRTM data can be used to determine the extent and topography of the dome shaped surface and a correlation was obtained between the convex peat dome surface and the depth of the underlying mineral ground, which was then used to calculate the peat volume and carbon store. The main problem of this approach was the determination of the vegetation height growing on top of the peat domes as the SRTM C-band sensor does not completely penetrate the forest cover. To get a high number of quality filtered footprints we investigated ICESat/GLAS data on peatlands for the whole of Kalimantan. The comparison of ICESat/GLAS elevations to the mean SRTM elevation showed a very high correlation of the waveform centroid ($R^2 = 0.92$). The mean ICESat/GLAS and SRTM elevation difference of -4.9 m (± 3.8 m) also showed that the SRTM C-band phase center penetration depth is dependent on forest structural parameters such as canopy closure. These results comply well with a study by Carabajal and Harding [53] and indicate that even for densely forested peat swamp areas the error is well below the 16 m at 90% confidence vertical

accuracy specifications for the SRTM mission. These findings demonstrate that with the help of ICESat/GLAS data the penetration depth of the SRTM C-band phase center into different peat swamp forest canopy closures and consequently the height of the SRTM elevation above the actual peat surface can be measured. Based on this it is reasonable to use ICESat/GLAS data as a tool to validate 3D peatland elevation models which were derived from SRTM data for selected regions in Central Kalimantan. Because the elevation from ICESat/GLAS last highest Gaussian peak is known to correspond best with the actual peat surface [22,28] we correlated it to the mean elevation of the three 3D peatland elevation models. Transects covering entire peat domes, clearly show the convex curvature of the peat domes (Figure 7(B)). The difference between the last highest Gaussian peak from the ICESat/GLAS data, referring to the estimated peat surface within the ICESat/GLAS waveform, and the 3D peatland elevation models, in which the forest canopy height was eliminated from the SRTM terrain model, was with -1.0 m (± 3.2 m) low. These results indicate that ICESat/GLAS data can be used to validate and enhance SRTM derived 3D peatland elevation models.

Furthermore, ICESat/GLAS data can be used as a sampling tool to screen for peatland areas in remote areas, such as West Papua. A systematic sampling with ICESat/GLAS could help to improve the knowledge on the spatial extent and curvature variation of peat domes and also consequently lead to better estimates of the carbon pools.

Considering peat swamp forest vertical structure we investigated specific ICESat/GLAS footprint transects in more detail that covered peat domes and adjacent areas where the land cover was known from optical satellite imagery and field surveys. Figure 7 shows one of these transects. From the elevation of the ICESat/GLAS signal begin, which corresponds to the top of the forest canopy, new and old burn scars, peat swamp forest fragments, logged and unlogged peat swamp forests are clearly discernible. Also apparent is a variation in the tree canopy height of the peat swamp forest which corresponds to different growth conditions in relation to hydrology. This leads to the conclusion that through combining optical data with ICESat/GLAS data it would be possible to obtain transect samples on the state and structure of peat swamp forests not only across the Indonesia archipelago but also in other regions where tropical peatlands occur.

Our field derived AGB values for tropical peat swamp forest lie in the range of existing literature values [54]. Different degradation levels between unlogged, logged and burned forests could be quantified. Most problematic were *in situ* tree height measurements as a multi-layered and dense canopy made it almost impossible to clearly sight tree tops. Especially in logged forest, dense undergrowth prevented from moving to a point where the tree top could be identified. Therefore we decided to use an allometric model for AGB calculation, which includes DBH and wood density but not tree height. The resulting correlation between field derived AGB values and airborne LiDAR data is comparable to other previously published values [52,55-59]. However, possible errors and limitations must be considered. For example errors might occur due to the use of a navigation GPS (C/A code only) for the forest sample plot locations, which had an accuracy of 3 to 10 m. Also effects like multi-path of the GPS signal in dense forested environments can lead to inaccurate location of the field plots. Due to these error sources the correlation might be influenced if the field plot location does not accurately match the location within the LiDAR 3D point cloud, which was measured more accurately by differential GPS. Also the filtering for ground points plays a key role. Peat swamp

forests grow on very flat terrain covered by tall forests with sometimes dense, scrubby undergrowth, which may impede the detection of the real soil surface. The error produced hereby and by the interpolation process could not be quantified because of a lack of reliable fine scale elevation data from the field. The resulting R^2 value of 0.75 ($n = 36$), where the average LiDAR point density per square meter was used as weighting factor in the linear regression, indicates that the established model should be valid, but the R^2 value is slightly lower than those reported for other biomes. LVIS (Laser Vegetation Imaging Sensor) data was successfully analyzed for forests in Costa Rica with a R^2 value of 0.89 [55]. Asner *et al.* [56] quantified AGB of a rain forest reserve on Hawaii Island using vertical profiles of a full waveform LiDAR system and showed that field-measured AGB was best predicted by the mean canopy height ($R^2 = 0.78$). Applying this approach in the Peruvian Amazon improved the resulting model ($R^2 = 0.85$) [57]. Analyzing discrete LiDAR data from a range of forest structural types in Australia Lucas *et al.* [58] derived a R^2 value of 0.92. A possible explanation for the lower R^2 value in our study could be that filtering for ground points is more erroneous in peat swamp forests. Preliminary results, where we investigated the same LiDAR data set in a lowland dipterocarp forest in Central Kalimantan resulted in a R^2 value higher than 0.90.

When correlating ICESat/GLAS elevations to airborne LiDAR 3D clouds and DTMs derived from these the signal begin and waveform centroid compared to the maximum z and mean z value all had R^2 values higher than 0.8, with the highest correlation between the waveform centroid and the mean z value ($R^2 = 0.91$, $n = 104$) (Table 1). The mean elevation difference between these two data sets was -0.5 m (± 1.9 m) for waveform centroid and the mean z value, 2.3 m (± 3.3 m) for the last highest Gaussian Peak and the minimum z value, and 3.2 m (± 3.2 m) for signal begin and the maximum z value. These results indicate that ICESat GLAS data and airborne LiDAR data comply well regarding elevation and that ICESat/GLAS data can be used as a tool to measure different elevations in these dense tropical peat swamp forest ecosystems. On the other hand when comparing ICESat/GLAS height metrics H1–H7 (Figure 2) to statistics from the normalized airborne LiDAR point clouds (z values of the airborne LiDAR points minus the corresponding DTM values) R^2 values were lower than 0.58 (Table 2). The highest R^2 were found when correlating percentile 95 with the ICESat/GLAS height metrics with exception of H7 (Figure 2) where percentile 80 had the highest R^2 value. The overall highest correlation ($R^2 = 0.57$, $n = 104$) was between 95% and ICESat/GLAS height metric H3 (Figure 2).

The best ICESat/GLAS AGB prediction model was achieved through a backward multiple regression approach with H1, H2, H4, H6, and H7 (Figure 2) as independent variables where the average LiDAR point density per square meter was ≥ 0.8 points ($R^2 = 0.61$, $n = 35$). The mean difference between the ICESat/GLAS AGB estimation and the airborne LiDAR AGB estimation was -2.62 ton 0.13 ha $^{-1}$ (± 10.78 ton 0.13 ha $^{-1}$, $n = 104$). For future studies it would be beneficial to have a higher number of ICESat/GLAS footprints intersecting with LiDAR point clouds with high average point densities. It has to also be considered that having multiple waveform derived variables (in our case 5) in the same equation may lead to collinearity problems. Comparing the model with other studies the R^2 value is in the lower range. Baccini *et al.* [21] found a strong positive correlation ($R^2 = 0.90$) between ICESat/GLAS height metrics and AGB values predicted from MODIS data across tropical Africa. Lefsky *et al.* [42] combined ICESat/GLAS waveforms and SRTM data to estimate maximum forest height in three ecosystems (tropical broadleaf forests in Brazil, temperate broadleaf forests in

Tennessee, and temperate needleleaf forests in Oregon). Additionally ICESat/GLAS derived heights for the Brazilian plots were correlated to AGB estimates from the field ($R^2 = 0.73$).

The results of our study demonstrate the usefulness and robustness of ICESat/GLAS data as a sampling tool to extract information on peatlands, which can be used as a proxy for peat volume and consequently carbon storage, state and structure of peat swamp forests, and peat swamp forest AGB for large inaccessible areas at low costs where no systematic sampling has been conducted yet. When combined with other data sources (optical satellite imagery, SRTM, and airborne LiDAR) ICESat/GLAS data can help to better understand carbon pools in tropical peatlands and their spatial distribution across Indonesia and other regions.

Acknowledgments

The authors would like to thank the National Snow and Ice Data Center for providing the ICESat/GLAS data. We would like to thank Suwido Limin and his team from the Centre for International Co-operation in Management of Tropical Peatland (CIMTROP) in Palangka Raya for the logistic support during the field inventory and Sampang Gaman (CIMTROP) and Simon Husson (Orangutan Tropical Peatland Project, OUTROP) for providing their tree species lists. Furthermore we would like to thank the Forest Restoration and Rehabilitation in Southeast Asia (FORRSA) project of the EU-funded Asia Link programme for financially supporting the field trip to Indonesia. The LiDAR data set was acquired by Kalteng Consultants.

References

1. Page, S.E.; Rieley, J.O.; Banks, C.J. Global and regional importance of the tropical peatland carbon pool. *Glob. Chang. Biol.* **2010**, *17*, 798-818.
2. Intergovernmental Panel on Climate Change. *Climate Change 2007: The Physical Science Basis. Contribution of Working Group I to the Fourth Assessment Report of the Intergovernmental Panel on Climate Change*; Solomon, S., Qin, D., Manning, M., Marquis, M., Averyt, K., Tignor, M.M.B., Miller, H.L., Jr., Chen, Z., Eds.; Cambridge University Press: Cambridge, UK, 2007.
3. Page, S.E.; Rieley, J.O. Tropical peatlands: A review of their natural resource functions with particular reference to Southeast Asia. *Int. Peat J.* **1998**, *8*, 95-106.
4. Sorensen, K.W. Indonesian peat swamp forests and their role as a carbon sink. *Chemosphere* **1993**, *27*, 1065-1082.
5. Rieley, J.O.; Ahmad-Shah, A.A.; Brady, M.A. The extent and nature of tropical peat swamps. In *Tropical Lowland Peatlands of Southeast Asia: Proceedings of a Workshop on Integrated Planning and Management of Tropical Lowland Peatlands held at Cisarua, Indonesia, 3–8 July 1992*; Maltby, E., Immirzi, C.P., Safford, R.J., Eds.; IUCN: Gland, Switzerland, 1996; pp. 17-53.
6. Anderson, J.A.R. *Ecosystems of the World 4b-Mires: Swamp, Bog, Fen and Moor*; Gore, A.J.P., Ed.; Elsevier: Amsterdam, The Netherlands, 1983; pp. 181-199.
7. Rieley, J.O.; Page, S.E. *Wise Use of Tropical Peatlands: Focus on Southeast Asia*; Rieley, J.O., Page, S.E., Eds.; ALTErrA: Wageningen, The Netherlands, 2005.

8. Page, S.E.; Wuest, R.A.J.; Weiss, D.; Rieley, J.O.; Shotyk, W.; Limin, S.H. A record of Late Pleistocene and Holocene carbon accumulation and climate change from an equatorial peat bog (Kalimantan, Indonesia): Implications for past, present and future carbon dynamics. *J. Quat. Sci.* **2004**, *19*, 625-635.
9. Hooijer, A.; Page, S.; Canadell, J.G.; Silvius, M.; Kwadijk, J.; Wösten, H.; Jauhiainen, J. Current and future CO₂ emissions from drained peatlands in Southeast Asia. *Biogeosciences* **2010**, *7*, 1505-1514.
10. Jaenicke, J.; Rieley, J.O.; Mott, C.; Kimman, P.; Siegert, F. Determination of the amount of carbon stored in Indonesian peatlands. *Geoderma* **2008**, *147*, 151-158.
11. Langner, A.; Miettinen, J.; Siegert, F. Land cover change 2002–2005 in Borneo and the role of fire derived from MODIS imagery. *Glob. Chang. Biol.* **2007**, *13*, 1-12.
12. ADB (Asian Development Bank)/BAPPENAS (National Development Planning Agency). *Causes, Extent, Impact and Costs of 1997/98 Fires and Drought Final report, Annex 1 and 2, Planning for Fire Prevention and Drought Management Project*; Asian Development Bank TA 2999-INO Fortech; Pusat Pengembangan Agribisnis, Margueles Pöyry: Jakarta, Indonesia, 1999.
13. Bompard, J.M.; Guizol, P. *Land Management in South Sumatra Province, Indonesia. Fanning the Flames: The Institutional Cause of Vegetation Fires*; European Union Forest Fire Prevention and Control Project and Indonesian Ministry of Forestry and Estate Crops: Jakarta, Indonesia, 1999.
14. Bowen, M.R.; Bompard, J.M.; Anderson, I.P.; Guizol, P.; Gouvon, A. *Forest Fires and Regional Haze in Southeast Asia*; Eaton, P., Radojevic, M., Eds.; Nova Science: New York, NY, USA, 2000; pp. 52-66.
15. Siegert, F.; Rücker, G.; Hinrichs, A.; Hoffmann, A. Increased fire impacts in logged over forests during El Niño driven fires. *Nature* **2001**, *414*, 437-440.
16. Langner, A.; Siegert, F. Spatiotemporal fire occurrence in Borneo over a period of 10 years. *Glob. Chang. Biol.* **2009**, *15*, 48-62.
17. Ballhorn, U.; Siegert, F.; Mason, M.; Limin, S. Derivation of burn scar depths and estimation of carbon emissions with LIDAR in Indonesian peatlands. *Proc. Nat. Acad. Sci. USA* **2009**, *106*, 21213-21218.
18. Page, S.E.; Siegert, F.; Rieley, J.O.; Boehm, H.-D.V.; Jaya, A.; Limin, S. The amount of carbon released from peatland forest fires in Indonesia during 1997. *Nature* **2002**, *420*, 61-65.
19. Ranson, K.J.; Kimes, D.; Sun, G.; Nelson, R.; Kharuk, V.; Montesano, P. Using MODIS and GLAS Data to Develop Timber Volume Estimates in Central Siberia. In *Proceedings of the IEEE International Geoscience and Remote Sensing Symposium, IGARSS 2007*, Barcelona, Spain, 23–28 July 2007; pp. 2306-2309.
20. Schutz, B.E.; Zwally, H.J.; Shuman, C.A.; Hancock, D.; DiMarzio, J.P. Overview of the ICESat Mission. *Geophys. Res. Lett.* **2005**, *32*, L21S01.
21. Baccini, A.; Laporte, N.; Goetz, S.J.; Sun, M.; Dong, H. A first map of tropical Africa's above-ground biomass derived from satellite imagery. *Environ. Res. Lett.* **2008**, *3*, 045011.
22. Boudreau, J.; Nelson, R.F.; Margolis, H.A.; Beaudoin, A.; Guindon, L.; Kimes, D.S. Regional aboveground forest biomass using airborne and spaceborne LiDAR in Quebec. *Remote Sens. Environ.* **2008**, *112*, 3876-3890.

23. Dolan, K.A.; Hurtt, G.C.; Chambers, J.Q.; Dubayah, R.O.; Frohling, S.; Masek, J.G. Using ICESat's Geoscience Laser Altimeter System (GLAS) to assess large-scale forest disturbance caused by hurricane Katrina. *Remote Sens. Environ.* **2011**, *115*, 86-96.
24. Goetz, S.J.; Sun, M.; Baccini, A.; Beck, P.S.A. Synergistic use of spaceborne lidar and optical imagery for assessing forest disturbance: An Alaska case study. *J. Geophys. Res.* **2010**, *115*, G00E07.
25. Harding, D.J.; Carajabal, C.C. ICESat waveform measurements of within footprint topographic relief and vegetation vertical structure. *Geophys. Res. Lett.* **2005**, *32*, L21S10.
26. Lefsky, M.A. A global forest canopy height map from the moderate resolution imaging spectroradiometer and the Geoscience Laser Altimeter System. *Geophys. Res. Lett.* **2010**, *37*, L15401.
27. Lefsky, M.A.; Keller, M.; Pang, Y.; de Camargo, P.B.; Hunter, M.O. Revised method for forest canopy height estimation from Geoscience Laser Altimeter System waveforms. *J. Appl. Remote Sens.* **2007**, *1*, 013537.
28. Rosette, J.A.B.; North, P.R.J.; Suarez, J.C. Vegetation height estimates for a mixed temperate forest using satellite laser altimetry. *Int. J. Remote Sens.* **2008**, *29*, 1475-1493.
29. Sun, G.; Ranson, K.J.; Kimes, D.S.; Blair, J.B.; Kovacs, K. Forest vertical structure from GLAS: An evaluation using LVIS and SRTM data. *Remote Sens. Environ.* **2008**, *112*, 107-117.
30. Page, S.E.; Rieley, J.O.; Shotyk, Ø.W.; Weiss, D. Interdependence of peat and vegetation in a tropical peat swamp forest. *Philos. Trans. R. Soc. B Biol. Sci.* **1999**, *354*, 1885-1897.
31. MacKinnon, K.; Hatta, G.; Halim, H.; Mangalik, A. *The Ecology of Kalimantan—Indonesian Borneo*; Periplus Editions (HK) Ltd.: Hong Kong, China, 1996.
32. Wetlands International. *Map of Peatland Distribution Area and Carbon Content in Kalimantan 2000–2002*; Wetlands International Indonesian Programme and Wildlife Habitat Canada: Bogor, Indonesia, 2004.
33. Moeliono, M.; Wollenberg, E.; Limberg, G. *The Decentralization of Forest Governance: Politics, Economics and the Fight for Control*; Earthscan: London, UK, 2009.
34. The National Snow and Ice Data Center, University of Colorado Boulder, Boulder, CO, USA, 2011. Available online: <http://nsidc.org/data/icesat/data.html> (accessed on 30 March 2011).
35. *NSIDC Distributed ICESat GLAS Laser Operations Periods: Latest Release*; The National Snow and Ice Data Center, University of Colorado Boulder, Boulder, CO, USA, 2011. Available online: http://nsidc.org/data/icesat/pdf/glas_laser_ops_attrib.pdf (accessed on 18 August 2011).
36. Rim, H.J.; Schutz, B.E. *Geoscience Laser Altimeter System (GLAS), Precision Orbit Determination (POD). Algorithm Theoretical Basis Documents (ATBD)*; Version 2.2; Center for Space Research, The University of Texas: Austin, TX, USA, 2002.
37. Bae, S.; Schutz, B.E. *Geoscience Laser Altimeter System (GLAS), Precision Attitude Determination (PAD). Algorithm Theoretical Basis Documents (ATBD)*; Version 2.2; Center for Space Research, The University of Texas: Austin, TX, USA, 2002.
38. Schutz, B.E. *Geoscience Laser Altimeter System (GLAS), Laser Footprint Location (Geolocation) and Surface Profiles. Algorithm Theoretical Basis Documents (ATBD)*; Version 3.0; Center for Space Research, The University of Texas: Austin, TX, USA, 2002.

39. Brenner, A.C.; Zwally, H.J.; Bentley, C.R.; Csatho, B.M.; Harding, D.J.; Hofton, M.A.; Minster, J.B.; Roberts, L.A.; Saba, J.L.; Thomas, R.H.; Yi, D. *Geoscience Laser Altimeter System (GLAS), Derivation of Range and Range Distributions from Laser Pulse Waveform Analysis for Surface Elevations, Roughness, Slope, and Vegetations Heights. Algorithm Theoretical Basis Documents (ATBD)*; Version 4.1; Center for Space Research, The University of Texas: Austin, TX, USA, 2003.
40. Ranson, K.J.; Sun, G.; Kovacs, K.; Kharuk, V.I. Landcover Attributes from ICESat GLAS Data in Central Siberia. In *Proceedings of the IEEE International Geoscience and Remote Sensing Symposium, IGARSS 2004*, Anchorage, AK, USA, 20–24 September 2004; Volume 2, pp. 753-756.
41. Ranson, K.J.; Sun, G.; Kovacs, K.; Kharuk, V.I. Use of ICESat GLAS Data for Forest Disturbance Studies in Central Siberia. In *Proceedings of the IEEE International Geoscience and Remote Sensing Symposium, IGARSS 2004*, Anchorage, AK, USA, 20–24 September 2004; Volume 3, pp. 1936-1939.
42. Lefsky, M.A.; Harding, D.J.; Keller, M.; Cohen, W.B.; Carabajal, C.C.; Del Bom Espirito-Santo, F.; Hunter, M.O.; de Oliveira, R., Jr. Estimates of forest canopy height and aboveground biomass using ICESat. *Geophys. Res. Lett.* **2005**, *32*, L22S02.
43. Lillesand, T.M.; Kiefer, R.W.; Chipman, J.W. *Remote Sensing and Image Interpretation*; John Wiley & Sons Inc.: Hoboken, NJ, USA, 2008.
44. Hansen, M.C.; DeFries, R.S.; Townshend, J.R.G.; Carroll, M.; Dimiceli, C.; Sohlberg, R.A. Global percent tree cover at a spatial resolution of 500 meters: First results of the MODIS Vegetation Continuous Fields Algorithm. *Earth Int.* **2003**, *7*, 1-15.
45. Pearson, T.; Walker, S.; Brown, S. *Sourcebook for Land Use, Land-Use Change and Forestry Projects*; Winrock International: Little Rock, AR, USA, 2005.
46. Chudnoff, M. *Tropical Timbers of the World*; Agriculture Handbook 607; US Department of Agriculture, Forest Service, Forest Products Laboratory: Madison, WI, USA, 1984.
47. *Wood Density Database*; World Agroforestry Centre: Nairobi, Kenya, 2011. Available online: <http://www.worldagroforestrycentre.org/Sea/Products/AFDbases/WD/Index.htm> (accessed on 30 March 2011).
48. Intergovernmental Panel on Climate Change. *2006 IPCC Guidelines for National Greenhouse Gas Inventories*; Eggleston, H.S., Buendia, L., Miwa, K., Ngara, T., Tanabe, K., Eds.; Prepared by the National Greenhouse Gas Inventories Programme; IGES: Hayama, Japan, 2006.
49. Brown, S. Estimating biomass and biomass change of tropical forests: A primer. *FAO For. Pap.* **1997**, *134*, 1-84.
50. Chave, J.; Andalo, C.; Brown, S.; Cairns, M.A.; Chambers, J.Q.; Eamus, D.; Fölster, H.; Fromard, F.; Higuchi, N.; Kira, T.; Lescure, J.-P.; Nelson, B.W.; Ogawa, H.; Puig, H.; Riera, B.; Yamakura, T. Tree allometry and improved estimation of carbon stocks and balance in tropical forests. *Oecologia* **2005**, *145*, 87-99.
51. Kraus, K.; Pfeifer, N. Determination of terrain models in wooded areas with airborne laser scanner data. *ISPRS J. Photogramm.* **1998**, *53*, 193-203.

52. Lefsky, M.A.; Cohen, W.B.; Harding, D.J.; Parkers, G.G.; Acker, S.A.; Gower, S.T. Lidar remote sensing of above-ground biomass in three biomes. *Glob. Ecol. Biogeogr.* **2002**, *11*, 393-399.
53. Carabajal, C.C.; Harding, D.J. SRTM C-band and ICESat laser altimetry elevation comparisons as a function of tree cover and relief. *Photogramm. Eng. Remote Sensing* **2006**, *72*, 287-298.
54. Waldes, N.J.L.; Page, S.E. Forest Structure and Tree Diversity of A Peat Swamp Forest in Central Kalimantan, Indonesia. In *Proceedings of the International Symposium on Tropical Peatlands*, Jakarta, Indonesia, 22–23 August 2001; pp. 16-22.
55. Drake, J.B.; Dubayah, R.O.; Clark, D.B.; Knox, R.G.; Blair, J.B.; Hofton, M.A.; Chazdon, R.L.; Weishampel, J.F.; Prince, S.D. Estimation of tropical forest structural characteristics using large-footprint lidar. *Remote Sens. Environ.* **2002**, *79*, 305-319.
56. Asner, G.P.; Hughes, R.F.; Varga, T.A.; Knapp, D.E.; Kennedy-Bowdoin, T. Environmental and biotic controls over aboveground biomass throughout a tropical rain forest. *Ecosystems* **2009**, *12*, 261-278.
57. Asner, G.P.; Powell, G.V.N.; Mascaro, J.; Knapp, D.E.; Clark, J.K.; Jacobson, J.; Kennedy-Bowdoin, T.; Balaji, A.; Paez-Acosta, G.; Victoria, E.; Secada, L.; Michael Valqui, M.; Hughes, R.F. High-resolution forest carbon stocks and emissions in the Amazon. *Proc. Nat. Acad. Sci. USA* **2010**, *107*, 16738-16742.
58. Lucas, R.M.; Cronin, N.; Lee, A.; Moghaddam, M.; Witte, C.; Tickle, P. Empirical relationships between AIRSAR backscatter and LiDAR-derived forest biomass, Queensland, Australia. *Remote Sens. Environ.* **2006**, *100*, 407-425.
59. Means, J.E.; Acker, S.A.; Harding, D.J.; Blair, J.B.; Lefsky, M.A.; Cohen, W.B.; Harmon, M.E.; McKee, W.A. Use of large-footprint scanning airborne lidar to estimate forest stand characteristics in the Western Cascades of Oregon. *Remote Sens. Environ.* **1999**, *67*, 298-308.

© 2011 by the authors; licensee MDPI, Basel, Switzerland. This article is an open access article distributed under the terms and conditions of the Creative Commons Attribution license (<http://creativecommons.org/licenses/by/3.0/>).